Seasonal mixed layer salinity balance of the tropical North Atlantic Ocean

Gregory R. Foltz[1] and Michael J. McPhaden[2]

[1]   In this study the causes of the seasonal cycle of mixed layer salinity in the tropical North Atlantic Ocean are investigated from a combination of satellite, atmospheric reanalysis, and in situ data sets. Results indicate that the salinity balance varies regionally, leading to a seasonal cycle in sea surface salinity (SSS) with significant spatial inhomogeneity. For example, horizontal salinity advection plays a key role in the salinity balance of the western tropical North Atlantic (10–25°N, 50–65°W), where seasonal variations in SSS are relatively large. In contrast, in the north-central basin (15–25°N, 20–50°W), freshening from meridional advection balances an excess of evaporation over precipitation, resulting in a very weak seasonal cycle of mixed layer salinity. Farther south (5–15°N, 20–45°W), seasonal variations of precipitation are more significant and drive a pronounced seasonal cycle of mixed layer salinity. Throughout most of the tropical North Atlantic the sum of the surface moisture flux and horizontal advection underestimates the mixed layer salinity tendency during boreal fall and winter. This is the time of year with highest wind speeds and highest negative buoyancy flux, suggesting that vertical turbulent entrainment of high-salinity thermocline water may be important. Daily measurements from a moored buoy in the central tropical North Atlantic are consistent with this interpretation. The results of this study highlight the complexity of the seasonal salinity balance in the tropical North Atlantic Ocean and the need for continued in situ monitoring of upper ocean salinity and currents to complement future space-based surface salinity measurements.

Citation: Foltz, G. R., and M. J. McPhaden (2008), Seasonal mixed layer salinity balance of the tropical North Atlantic Ocean, *J. Geophys. Res.*, *113*, C02013, doi:10.1029/2007JC004178.

1.   Introduction

[2]   Salinity plays an important role in tropical climate through its effects on upper ocean stratification. Significant salinity stratification within a deeper isothermal layer can generate a "barrier layer" between the base of the isothermal layer and the base of the mixed layer [*Lukas and Lindstrom*, 1991; *Sprintall and Tomczak*, 1992]. Barrier layers affect sea surface temperatures (SST) by reducing the entrainment of cool thermocline water into the mixed layer. They also affect currents by trapping momentum input from the wind in a shallow surface layer, thereby producing strong surface flows [e.g., *Vialard and Delecluse*, 1998].

[3]   One of the regions where these effects are likely to be important is the tropical North Atlantic. This region is characterized by strong river discharge, seasonally varying precipitation, and southward subduction of high-salinity water from the subtropical North Atlantic. All of these factors contribute to the formation of significant (thickness >10 m), seasonally varying barrier layers that impact local SST [*Sprintall and Tomczak*, 1992; *Pailler et al.*, 1999; *Ffield*, 2007] (Figure 1). Changes in SST in the tropical North Atlantic in turn affect rainfall in Northeast Brazil and sub-Saharan Africa [*Lamb*, 1978; *Hastenrath and Greischar*, 1993; *Giannini et al.*, 2003] and tropical cyclone formation and intensification within the Atlantic basin [*Saunders and Harris*, 1997; *Shapiro and Goldenberg*, 1998; *Goldenberg et al.*, 2001; *Latif et al.*, 2007].

[4]   Previous observational efforts to understand the seasonal cycle of sea surface salinity (SSS) in the tropics have focused mainly on the Pacific and Indian Oceans or on large-scale, global analyses [e.g., *Delcroix and Hénin*, 1991; *Delcroix et al.*, 1996; *Cronin and McPhaden*, 1998; *Johnson et al.*, 2002; *Rao and Sivakumar*, 2003]. A common theme among all of these studies is the importance of precipitation and horizontal salt advection in the seasonal salinity balance. Analyses of the seasonal salinity balance in the tropical Atlantic are more limited in comparison to those in the other tropical oceans. *Dessier and Donguy* [1994] analyzed SSS measurements from ships of opportunity and research vessels and found a pronounced seasonal cycle of SSS throughout most of the tropical North Atlantic. They concluded that SSS variability in the western tropical North Atlantic is governed mainly by freshwater outflow from the Amazon and Orinoco

[1]Joint Institute for the Study of the Atmosphere and Ocean, University of Washington, Seattle, Washington, USA.
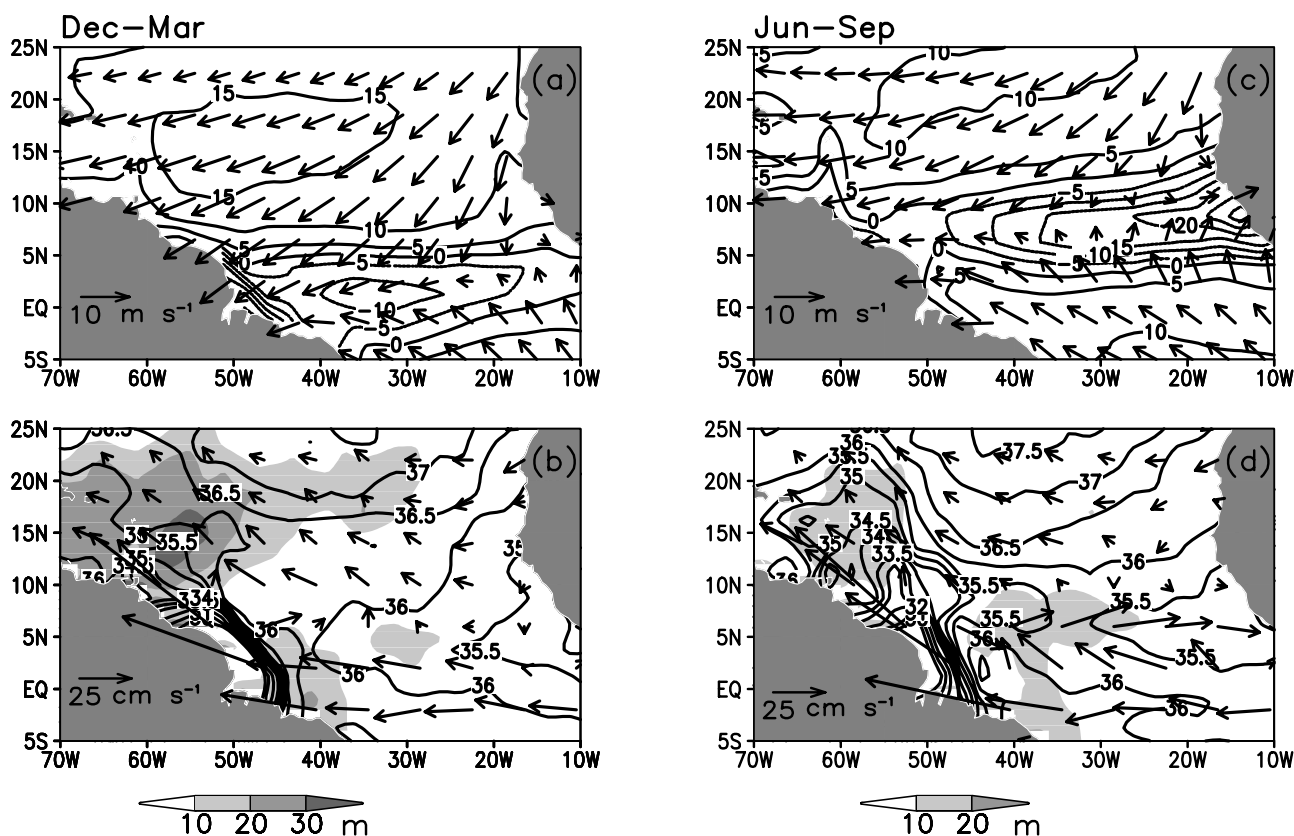[2]Pacific Marine Environmental Laboratory, NOAA, Seattle, Washington, USA.

Figure 1. (a) Mean December–March evaporation-minus-precipitation (cm month^{-1}, contours) and surface winds (arrows). (b) December–March surface salinity (contours, psu), near-surface currents (vectors), and barrier layer thickness (shading). (c and d) Same as Figures 1a and 1b except for June–September.

Rivers and that variability in the central basin is driven primarily by changes in the surface moisture flux (evaporation minus precipitation; E−P). *Foltz et al.* [2004] examined the causes of the seasonal cycle of mixed layer salinity at four Pilot Research Moored Array in the Tropical Atlantic (PIRATA) locations along 38°W. They found that the seasonal cycle of mixed layer salinity along this meridian is balanced to a large extent by seasonal variations of horizontal salinity advection and precipitation.

[5] Both of the aforementioned studies were limited by data availability. The basin-scale analysis of *Dessier and Donguy* [1994] did not explicitly estimate the contributions from horizontal or vertical salinity advection. In contrast, the study of *Foltz et al.* [2004] presented a more detailed mixed layer salinity analysis that nevertheless was limited to four mooring locations at a single longitude. As a result, there remains considerable uncertainty regarding the causes of the seasonal cycle of SSS in the tropical North Atlantic. In this study we combine satellite, in situ, and atmospheric reanalysis products to diagnose the seasonal cycle of mixed layer salinity in the tropical North Atlantic, expanding on the results of *Dessier and Donguy* [1994] and *Foltz et al.* [2004].

2. Data and Methods

2.1. Data Sets

[6] We combine salinity measurements from a variety of sources in order to generate a seasonal climatology of SSS.

Surface salinity data from various sources have been merged successfully in several previous studies, primarily for examining variability in the Pacific Ocean or for statistical analyses along ship tracks in the Atlantic [e.g., *Delcroix et al.*, 1996, 2005; *Maes et al.*, 2006]. A global objectively analyzed monthly climatology of surface salinity is available from the World Ocean Atlas 2001 (WOA01 [*Boyer et al.*, 2002]). However, this data set does not include surface measurements from ships of opportunity, which comprise a significant portion of the historical database in the tropical North Atlantic (Figure 2). We have therefore created a monthly climatological SSS data set from the combination of measurements from ships, World Ocean Database 2001 (WOD01), Argo, and PIRATA moorings.

[7] SSS samples have been collected by research vessels and ships of opportunity in the tropical Atlantic since 1977 [*Dessier and Donguy*, 1994]. The samples are collected every 3–6 h, giving a spatial resolution of 0.5–2° along ship tracks and an accuracy of ∼0.1 psu [*Reverdin et al.*, 1994]. Beginning in 1995 thermosalinograph (TSG) measurements began to replace bucket sampling. Measurements are made every 15 s, and median values over 5 min are recorded, giving an along-track resolution of ∼0.02° and an accuracy of ∼0.02 psu [e.g., *Hénin and Grelet*, 1996]. The bucket and TSG data sets are available for 1989–2006 from the Global Ocean Surface Underway Data (GOSUD) pilot
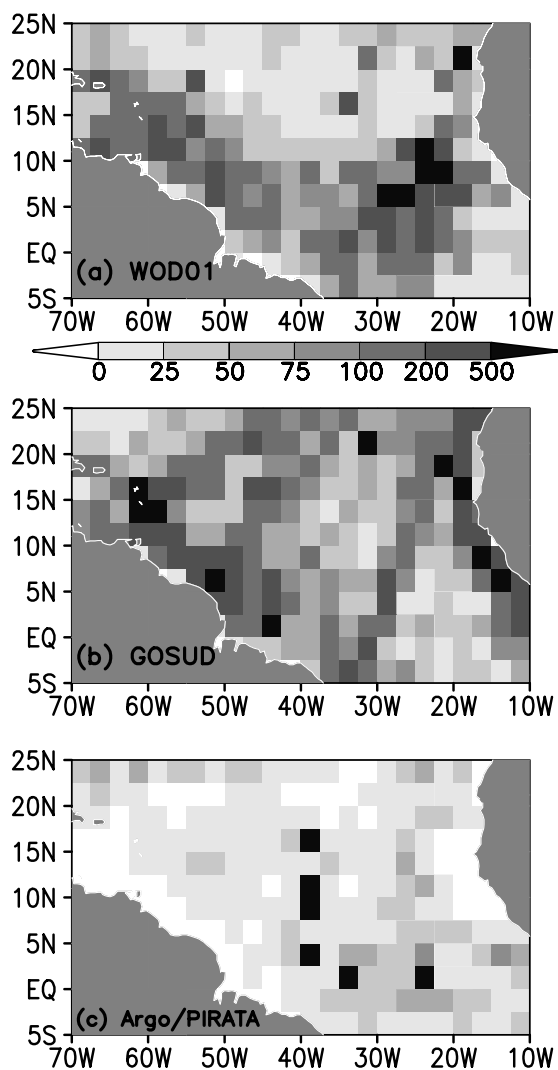
Figure 2. Total number of surface salinity measurements from (a) World Ocean Database 2001, (b) Global Ocean Surface Underway Data project (GOSUD), and (c) the combination of Argo and PIRATA.

project (ftp://ftp.ifremer.fr/ifremer/gosud). The analysis of *Delcroix et al.* [2005] suggests that there are ∼5 (6) independent SSS samples in each 2° north−south (east−west) transect, corresponding to a sampling interval of ∼2 h. Since our gridding procedure (described later in this section) estimates SSS in 2.5° × 2.5° grid boxes, we average all bucket and TSG data to 2-h means.

[8] We also use SSS data from bottle samples and conductivity-temperature-depth (CTD) profiles that are available from WOD01 [*Conkright et al.*, 2002] beginning in the early 1900s and from Argo floats beginning in 2000 [*Roemmich*, 2000]. Argo data include both real-time and delayed mode salinity profiles that have passed the corresponding quality control tests at all depth levels [*Wong et al.*, 2003]. Argo and WOD01 profiles are vertically and linearly interpolated to a depth of 5 m, and this value is used as an estimate of SSS. Since 1998 salinity measurements have been available from the PIRATA moorings at depths of 1 m, 20 m, 40 m, and 120 m [*Servain et al.*, 1998]. These data have an accuracy of 0.02 psu [*Freitag et al.*, 1999] and

a decorrelation timescale of ∼2 d [*Delcroix et al.*, 2005]. We therefore average all PIRATA salinity data to 2-d means and use measurements from a depth of 1 m as estimates of SSS.

[9] Our analysis procedure begins with the removal of duplicate data and data with values <20 psu or >40 psu. We then collect all SSS measurements in 2.5° × 2.5° bins for each climatological month and remove values that are not within three quartiles of the median in each monthly grid box. The individual SSS data are then interpolated onto a 2.5° × 2.5° grid for each climatological month using objective analysis (see Appendix A).

[10] We use a variety of other data sets in addition to the SSS climatology described above. These include the monthly climatological mixed layer depth (MLD) estimates of *de Boyer Montégut et al.* [2007] (hereinafter referred to as BM07) and *Monterey and Levitus* [1997] (hereinafter referred to as ML97). The BM07 data set is based on vertical temperature and salinity profiles from WOD01 and Argo, and the ML97 MLD is based on World Ocean Database 1994 (WOD94) temperature and salinity profiles. The typical vertical resolution of the WOD94, WOD01, and Argo profiles near the surface is 5 m. The BM07 data set is available on a 2° × 2° grid and the ML97 data set on a 1° × 1° grid. The BM07 MLD estimates are based on the criterion of the density equivalent of a 0.2°C temperature decrease from a depth of 10 m (generally ∼0.07 kg m^{-3} in the tropical North Atlantic) using individual temperature and salinity profiles, whereas ML97 use a 0.125 kg m^{-3} density increase from the surface from objectively analyzed fields. BM07 found that the criterion of the density equivalent of a 0.2°C temperature decrease from 10 m is small enough to capture the seasonal variations of MLD but large enough to avoid aliasing the effects of the diurnal cycle. In contrast, the ML97 criterion may be contaminated by measurements of the shallow diurnal warm layer since it uses surface reference values. Indeed, ML97 estimates are 0−15 m shallower than BM07 estimates throughout most of the tropical North Atlantic.

[11] We also obtained the monthly climatological barrier layer thickness (BLT) data set of BM07. The BLT is defined as the difference between the isothermal layer depth, calculated using the criterion of a 0.2°C decrease from a depth of 10 m, and the mixed layer depth. This data set is used only to examine the large-scale climatological conditions in the tropical North Atlantic (Figure 1) and is not used in the salt budget analysis described later in this section.

[12] Monthly mean estimates of surface evaporation are obtained from a combined satellite/reanalysis product on a 1° × 1° grid for the time period 1981−2002 [*Yu et al.*, 2004] and from the International Comprehensive Ocean-Atmosphere Data Set (ICOADS [*Worley et al.*, 2005]) on a 1° × 1° grid for the period 1960−2002. The reanalysis products in the *Yu et al.* [2004] analysis consist of the NCEP/DOE reanalysis-2 (hereinafter NCEP2 reanalysis [*Kanamitsu et al.*, 2002]) and the ECMWF 40-year reanalysis [*Simmons and Gibson*, 2000]. Surface turbulent fluxes were computed from these products using daily mean wind speed, SST, and humidity in the bulk flux algorithm developed from the Coupled Ocean-Atmosphere Response Experiment (COARE [*Fairall et al.*, 2003]). The ICOADS data set consists of ship observations of the latent heat flux param-

eter, $W(q_s - q_a)$, where W is wind speed, q_s is saturation specific humidity, and q_a is air specific humidity. We use the *Fairall et al.* [2003] algorithm to estimate the total latent heat flux and evaporation from the flux parameter. Because the *Yu et al.* [2004] product incorporates satellite and reanalysis data, it provides extensive spatial and temporal coverage. In contrast, ICOADS suffers from significant data gaps, but has the advantage of using direct measurements for latent heat flux calculations. For each data set we form a monthly mean climatology using all available data.

[13] We use three different precipitation data sets in this study. Monthly mean estimates are obtained from the Global Precipitation Climatology Project (GPCP [*Adler et al.*, 2003]) and the Climate Prediction Center's Merged Analysis of Precipitation (CMAP [*Xie and Arkin*, 1997]). Both use measurements from rain gauges and from satellite infrared and microwave sensors and are available for 1979–2006 on a 2.5° × 2.5° grid. The two products differ primarily in the methodologies used to combine the in situ and satellite data sets. The third precipitation data set we use consists of monthly mean precipitation estimates from the Microwave Imager and Precipitation Radar onboard the Tropical Rainfall Measuring Mission satellite (TRMM). These data are available on a 0.5° × 0.5° grid for 1998–2006 and are not included in the GPCP and CMAP analyses. For each product we form a monthly climatology from all available data to maximize the number of realizations of the mean seasonal cycle.

[14] We obtained three different estimates of horizontal mixed layer velocity. One calculates currents at an average depth of ~15 m using velocity estimates from surface drifters and ship drifts, together with satellite-based sea level and wind stress [*Grodsky and Carton*, 2001]. These data are available as a monthly climatology on a 2°-lat × 3°-lon grid. The second uses near-surface velocity from satellite-tracked drifting buoys and is available as a monthly mean climatology on a 1° × 1° grid [*Lumpkin and Garzoli*, 2005]. Finally, we obtained estimates of horizontal velocity averaged in the upper 30 m from the Ocean Surface Current Analysis–Realtime (OSCAR [*Bonjean and Lagerloef*, 2002]). This method uses satellite sea level, wind stress, and SST, together with a diagnostic model, to calculate velocity on a 1° × 1° × 5-d grid for the time period 1993–2006. The OSCAR product has the advantage of more complete spatial and temporal coverage than the ship drift and drifter-based climatologies because it uses satellite measurements, but has the disadvantage of not being constrained by direct velocity observations.

[15] We use a number of data sets to assess the role of mixed layer turbulence generation and vertical entrainment in the salinity balance (described in section 4). These include monthly estimates of NCEP2 reanalysis wind speed and net surface longwave radiation emission for the time period 1983–2002, and the *Yu et al.* [2004] surface latent and sensible heat flux and *Zhang et al.* [2004] surface shortwave radiation for the same time period. The Zhang et al. data set uses cloud properties from the International Satellite Cloud Climatology Project (ISCCP) combined with a radiative transfer model and is available on a 2.5° × 2.5° grid. Climatological subsurface salinity data were obtained from WOA01 on a 1° × 1° grid at a vertical resolution of 10 m in the upper 30 m and 25 m between 50 m and 150 m.

[16] Finally, we use data from the PIRATA moorings at 15°N, 12°N, and 8°N along 38°W to estimate entrainment (see section 4) and to estimate uncertainties associated with the evaporation and precipitation products described previously in this section (see Appendix A). Measurements at these locations, begun in 1998 and continued through the present, include subsurface temperature and salinity, air temperature, relative humidity, wind velocity, shortwave radiation, and precipitation. From 1998 to June 2005, ocean temperature was measured at 11 depths between 1 m and 500 m, with 20-m spacing in the upper 140 m, while salinity was measured at 1 m, 20 m, 40 m, and 120 m at all moorings. Beginning in July 2005, additional temperature measurements have been made at 10 m and 13 m and additional salinity measurements at 10 m and 60 m at the 15°N, 38°W mooring. Air temperature and relative humidity are measured at a height of 3 m above sea level, shortwave radiation and rainfall are measured at 3.5 m, and wind velocity at 4 m. Daily averages are transmitted to shore in real-time, while high temporal resolution data (1 to 10 min averages) are internally recorded. Here we use the daily averaged data for the time period January 1998 to October 2006.

[17] All of the aforementioned monthly climatologies were regridded to a 2.5°-lat × 2.5°-lon grid for consistent analysis across all fields. We use the combined ship/ WOD01/Argo/ PIRATA SSS analysis together with GPCP precipitation, *Yu et al.* [2004] evaporation, BM07 MLD, and *Grodsky and Carton* [2001] velocity estimates in an initial analysis of the mixed layer salinity balance in the tropical North Atlantic. The other data sets described above are then used to estimate entrainment and to assess uncertainties in the salinity budget.

2.2. Methodology

[18] To address the causes of the seasonal cycle of surface salinity in the tropical North Atlantic we consider the mixed layer salinity equation

$$\frac{\partial S}{\partial t} = \frac{(E - P)S}{\rho h} - \mathbf{v} \cdot \nabla S + \epsilon \qquad (1)$$

[19] The terms in (1) represent, from left to right, mixed layer salinity tendency, surface freshwater flux, horizontal advection, and the sum of terms that we cannot reliably estimate. Here h is the depth of the mixed layer, S and $\mathbf{v}$ are salinity and horizontal velocity, respectively, vertically averaged from the surface to a depth of $-h$, E is evaporation, and P is precipitation.

[20] Mixed layer salinity tendency is estimated using the monthly gridded SSS as a substitute for S. We have found that differences between S and SSS are generally small in comparison to seasonal variations of SSS, based on measurements from the PIRATA moorings at 8°N, 12°N, and 15°N along 38°W. Monthly climatological RMS differences between S and SSS are 0.05, 0.04, and 0.03 psu at 8°N, 12°N, and 15°N, respectively. Differences are significantly reduced when higher vertical resolution temperature and salinity data from WOA01 are used to estimate S (RMS differences are 0.03, 0.02, and 0.01 at 8°N, 12°N, and 15°N, respectively). Maximum differences at all locations tend to occur when the barrier layer is thickest, which is during
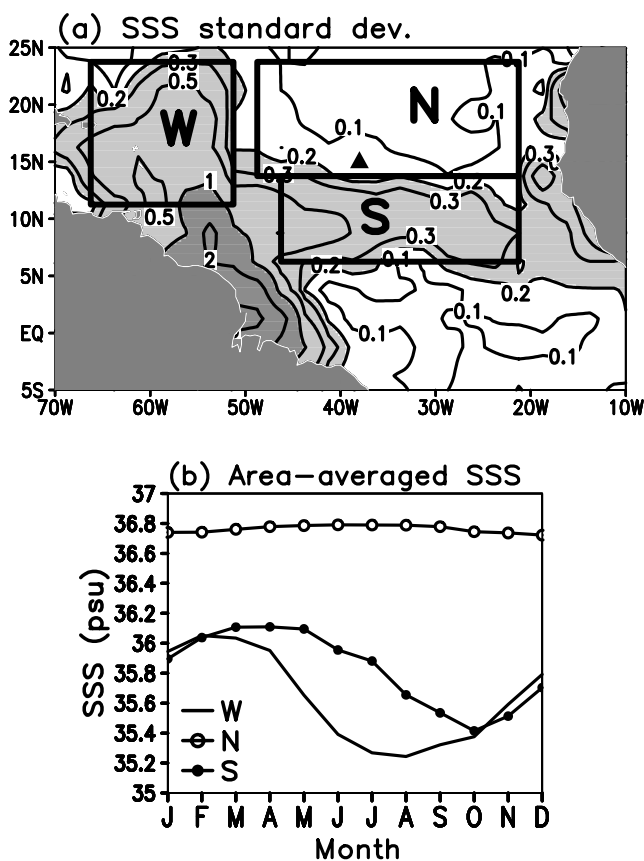
Figure 3. (a) Standard deviation of monthly climatological SSS (contours; light shading >0.2 psu, dark shading >1 psu). Boxes denote averaging regions for Figures 4−9; solid triangle indicates position of the PIRATA mooring used in this study. (b) Seasonal cycle of SSS in each of the regions shown in Figure 3a.

boreal fall at 8°N and 12°N and boreal winter at 15°N [*Foltz et al.*, 2004].

[21] The residual (ϵ) likely consists mainly of the combination of entrainment, vertical turbulent diffusion, and horizontal eddy advection. The potential role of entrainment in the salinity balance is discussed in section 4. For all terms in (1) we form monthly climatologies and smooth with a 3-month running mean filter. We estimate errors for each term in (1) on the basis of uncertainties in the estimation of SSS, MLD, mixed layer currents, evaporation, and precipitation (see Appendix A and section 4).

[22] In order to increase the statistical reliability of our calculations, we consider the mixed layer salinity balance averaged in three regions of the tropical North Atlantic (western (W), northern (N), and southern (S); Figure 3a). The W and S boxes encompass regions with strong seasonal SSS variability (standard deviation >0.2 psu), while the N box encompasses a region with much weaker variability in comparison. The W region is influenced by the transport of relatively fresh water from the south and is characterized by a thick barrier layer during boreal winter (Figure 1b). The northern box (N) bounds a region of high annual mean SSS (>37 psu) that is located north of the climatological position of the ITCZ. SSS in this region exhibits almost no seasonal

cycle despite changes in E−P of ∼5 cm month^{-1} (Figures 1a and 1c).

[23] The southern tropical North Atlantic (box S in Figure 3a) is more strongly influenced by ITCZ precipitation than either the W or N regions and additionally exhibits significant seasonal variability of the zonal mixed layer currents. Our choice of the bounds for region S was influenced by the presence of a sharp, meridionally oriented, SSS front near 45°W (Figure 1). The combination of the SSS front and strong zonal currents (monthly mean values of ∼40 cm s^{-1} during boreal fall) leads to large uncertainties in our estimates of zonal mixed layer salinity advection west of ∼45°W. We therefore focus on the central ITCZ region to the east of this meridian.

3. Results

[24] Before considering the mixed layer salinity balance in detail, we examine the surface oceanic and atmospheric fields in the tropical North Atlantic. Seasonal variations of the surface moisture flux (E−P) reflect seasonal changes in the position and intensity of the band of high precipitation associated with the intertropical convergence zone (ITCZ). During boreal winter and spring the ITCZ is farthest south and E−P < 0 in the 0−5°N latitude band. The northeasterly trade winds are strongest in these seasons, driving a maximum in evaporation in the 10−20°N latitude band (Figure 1a). The ITCZ moves northward and intensifies in boreal summer. The strongest precipitation shifts eastward toward the African coast, and evaporation weakens north of the ITCZ (Figure 1c).

[25] The dominant source of freshwater runoff in the tropical North Atlantic is the Amazon River. Outflow from the Amazon reaches a minimum in boreal fall and winter [*Dai and Trenberth*, 2002], coinciding with a maximum in SSS throughout the western basin (Figure 1b). Surface currents are mainly westward during these seasons so that outflow is confined near the coast of South America. Freshwater runoff peaks in May−June, contributing to a large pool of low-salinity water in the western tropical North Atlantic (Figure 1d). Zonal surface currents reverse and intensify during boreal summer, transporting low-salinity water eastward from the mouth of the Amazon in the 5−10°N latitude band [*Muller-Karger et al.*, 1988].

[26] In response to changes in E−P, river runoff, and oceanic circulation, seasonal SSS variability is strongest near the mouth of the Amazon, with a secondary maxima in the northwestern basin and in a zonal band centered near 10°N (Figure 3a). The secondary maximum in the northwestern basin is associated with the expansion and contraction of the Amazon plume, and the local maximum in the central basin roughly coincides with the northernmost extent of the ITCZ. Surface salinity variability is weakest in the subtropical North Atlantic, where the annual mean SSS is high and the seasonal cycle of precipitation is weak (Figures 1 and 3).

[27] Next we consider the mixed layer salinity balances in the three regions shown in Figure 3, beginning in the west. In the W region, SSS reaches a maximum in boreal winter (>36 psu), then decreases rapidly during boreal spring to a minimum of ∼35.2 psu in July and August (Figure 3b). The period of significant freshening during boreal spring is
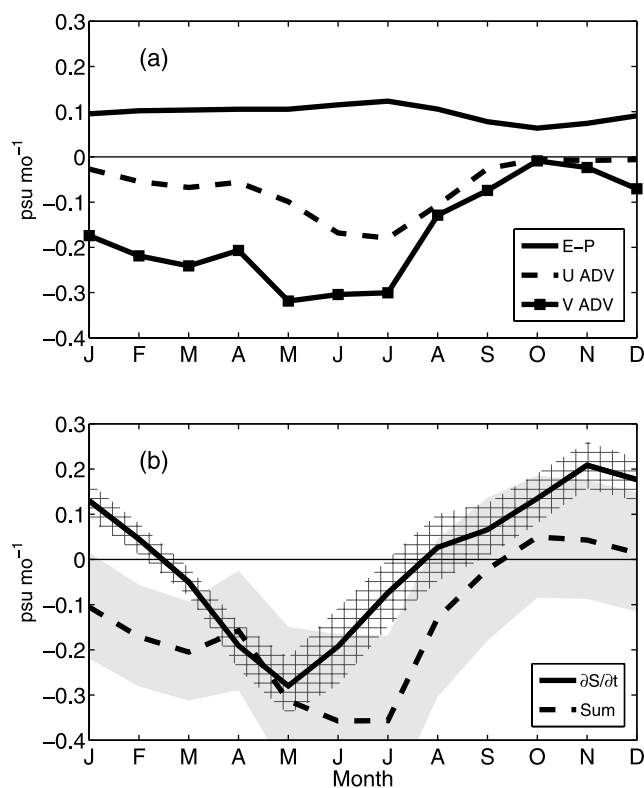
Figure 4. (a) Terms in the mixed layer salt balance in the W region (see Figure 3a for bounds of the region): surface moisture flux (E−P), zonal advection (U ADV), and meridional advection (V ADV). (b) Sum of the terms in Figure 4a (dashed) and the mixed layer salt storage rate (solid). Shading and hatching are one standard error for the sum and storage, respectively (described in Appendix A).

caused by the northwestward advection of low-salinity water from the Amazon (Figure 4). Meridional advection dominates zonal advection during the first half of the year because of a stronger meridional SSS gradient (Figure 5). The maxima in meridional velocity and $\partial S/\partial y$ and the corresponding minimum of meridional advection (maximum freshening) during May−July occur ~1 month after the maximum in Amazon River discharge to the south. Zonal advection provides freshening throughout the year in the W region, with a seasonal cycle that is in phase with that of meridional advection (Figure 4a). The minimum in zonal advection during June−July coincides with maxima in westward mixed layer velocity and the negative SSS gradient in the southern portion of the W region (south of 15°N; Figure 5).

[28] The seasonal cycle of E−P is considerably weaker than that of either component of horizontal advection. As a result, changes in mixed layer salinity in the W region are driven primarily by changes in horizontal advection. The sum of the E−P and horizontal advection terms underestimates the mixed layer salinity tendency throughout most of the year, however, suggesting that unresolved processes, such as entrainment and eddy advection may also be important (see section 4).

[29] Next we consider the salinity balance in the northern tropical Atlantic (box N in Figure 3a). This region is

characterized by higher annual mean SSS and a much weaker seasonal cycle in comparison to the western tropical North Atlantic (Figure 3b). The positive salinity tendency induced by an excess of evaporation over precipitation is balanced by the northward transport of fresher water from the region underlying the mean position of the ITCZ (Figure 6). As a result, the seasonal cycle of mixed layer salinity tendency is close to zero throughout the year. The annual mean and seasonal variability of meridional mixed layer velocity and $\partial S/\partial y$ are weaker in this region in comparison to the W region, explaining the weaker annual mean and seasonal amplitude of meridional advection in the N region. There is a weak maximum in the amplitude of meridional advection during boreal winter that is associated with corresponding maxima in northward velocity and $\partial S/\partial y$.

[30] Seasonal variability of SSS increases southward from the subtropical North Atlantic, reaching a maximum near 10°N (Figure 3a). The enhanced variance in this region (box S in Figure 3a) relative to that in the N region results mainly from an enhancement of the seasonal cycle of E−P in the S region (Figure 7a). Precipitation reaches a maximum during August−September, when the ITCZ is farthest north (Figure 1c), driving a freshening tendency of mixed layer salinity in the S region (Figure 7). During boreal winter E−P reverses sign, tending to increase mixed layer salinity. However, E−P at this time is balanced to a large extent by freshening due to northward currents in the presence of a positive SSS gradient. As a result, the sum of the forcing terms predicts only a weak increase in salinity during boreal winter, whereas the actual mixed layer salinity increases more substantially (Figure 7b). Zonal advection is weak throughout the year in the S region, whereas the results of *Muller-Karger et al.* [1988] imply significant eastward transport of low-salinity water from the Amazon in the 5−10°N latitude band during boreal summer and fall. The observational analysis of *Foltz et al.* [2004] also suggests that zonal advection provides a significant source of freshening at 8°N, 38°W during August−November. The difference between our results and those of *Muller-Karger et al.* [1988] and *Foltz et al.* [2004] relates to our large zonal average (over 25° of longitude), which smears out some of the zonal advective effects that would be evident on smaller spatial scales.

4. Residual

4.1. Data Dependence

[31] In boreal winter the sum of evaporation, precipitation, and horizontal advection underestimates the mixed layer salinity tendency by ~0.1 psu month^{-1} in the N region and by ~0.2 psu month^{-1} in the W and S regions (Figures 4b, 6b, and 7b). There are several possible explanations for these discrepancies, one class of which relates to errors in the data sets we have used. First, there are uncertainties in our estimates of precipitation. In an attempt to better quantify these uncertainties, we have compared monthly climatologies from GPCP, CMAP, and TRMM. Differences between the SSS tendencies from GPCP and CMAP are <0.03 psu month^{-1} throughout the year in the W and N regions and are <0.05 psu month^{-1} in the S region. Maximum discrepancies occur in September−October, when climatological precipitation is greatest. In all three
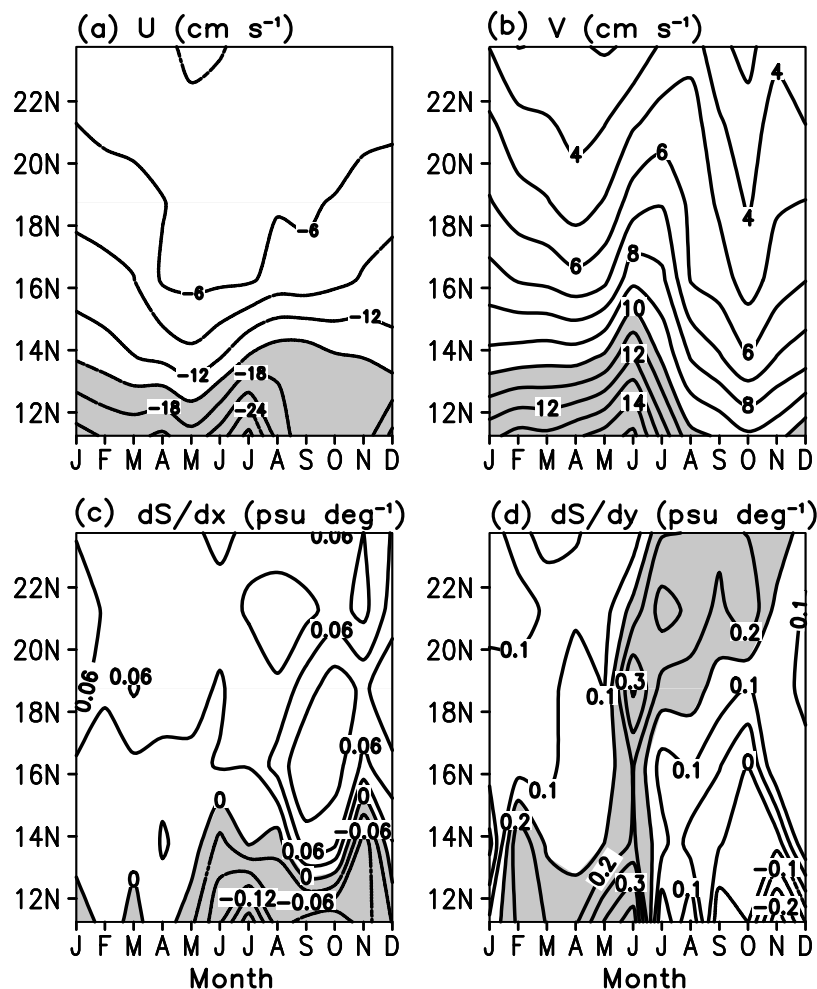
Figure 5. Latitude-time plots of (a) zonal and (b) meridional mixed layer velocity and (c) zonal and (d) meridional salinity gradient averaged zonally in the W region. Shading in Figures 5a and 5b emphasizes strong westward (>15 cm s^{-1}) and northward (>10 cm s^{-1}) velocity, respectively. Shading in Figures 5c and 5d emphasizes strong westward (>0.03 psu deg^{-1}) and northward (>0.15 psu deg^{-1}) SSS gradients, respectively.

regions CMAP estimates are higher, consistent with the analysis of *Yin et al.* [2004]. The residuals in the salinity balance are therefore larger in all regions if CMAP data are substituted for GPCP. Absolute differences in SSS tendencies due to GPCP and TRMM are smaller (<0.02 psu month^{-1} in the W, N, and S regions), with TRMM estimates generally higher. It is therefore unlikely that uncertainties in precipitation can explain the residuals in the W, N, and S regions, which indicate a missing source of salt.

[32] It is also unlikely that uncertainties in evaporation contribute significantly to the residuals. We have compared the *Yu et al.* [2004] and ICOADS monthly climatologies of evaporation and found differences in inferred SSS tendencies of <0.02 psu month^{-1} (ICOADS estimates are higher). Maximum differences occur in boreal spring/summer, when the residuals in the area-averaged salinity balances are smallest. Substitution of ICOADS evaporation into the salinity balance in the N region results in a significant negative residual during May−July of ∼0.02 psu month^{-1} (i.e., the sum of horizontal advection and E−P exceeds the

salinity storage rate). In the W and S regions the residuals are not changed significantly.

[33] The salinity balance is also affected by the criterion used to estimate mixed layer depth (MLD). In an attempt to quantify this sensitivity, we have compared the monthly climatological MLD estimates of BM07 to those of ML94.Throughout the tropical North Atlantic ML94 estimates are 0−15 m shallower than those of BM07. The differences are largest in boreal winter, when the MLD is deepest (40−65 m). The only term in the salinity balance that is affected by changes in MLD is the surface moisture flux (E−P; equation (1)). Substitution of ML94 MLD into the salinity balance results in a ∼0.1 psu month^{-1} increase in the E−P term in the W region and a ∼0.02 psu month^{-1} increase in the N region, reducing the storage-sum residuals in both regions to within the errors bars of our calculations. It is therefore possible that uncertainties in MLD may contribute significantly to the residual in the W and N regions. In the S region substitution of the ML97 MLD increases the magnitude of the E−P term by ∼0.1 psu month^{-1} during July−October, when precipitation is stron-
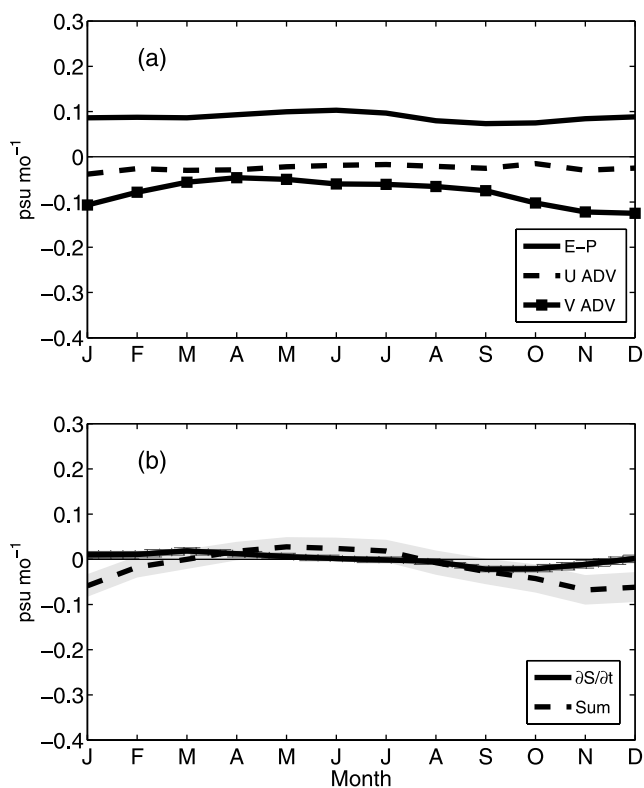
Figure 6. Same as in Figure 4 except for the N region (see Figure 3a for bounds of the region).

gest. This results in an increase in the magnitude of the residual during these months. During January–April, when E−P > 0 in the S region, substitution of ML97 MLD reduces the residual by ~0.02 psu month[−1]. Since the magnitude of the residual is >0.1 psu month[−1] during these months, it is unlikely that uncertainties in MLD alone can account for our inability to close the salinity budget.

[34] There are also uncertainties in our estimation of horizontal advection that are due to a combination of uncertainties in horizontal mixed layer salinity gradients and mixed layer velocity. We have compared estimates of horizontal mixed layer salinity advection using the *Grodsky and Carton* [2001] (hereinafter referred to as GC01) currents to estimates from OSCAR and from the surface drifter climatology of *Lumpkin and Garzoli* [2005] (hereinafter referred to as LG05). Horizontal advection based on GC01 and LG05 currents agree reasonably well throughout the tropical North Atlantic, with discrepancies of at most 0.1 psu month[−1] (Figure 8). Substitution of LG05 currents for GC01 currents does not significantly affect the residual in either the W, N, or S region. In contrast, OSCAR currents are consistently weaker than GC01 and LG05 currents throughout the tropical North Atlantic (Figure 8). This is consistent with the analysis of *Johnson et al.* [2007], which found that OSCAR underestimates horizontal velocity poleward of 10° of latitude. Differences are largest in the W region, where both GC01 and LG05 currents predict freshening of 0.2–0.6 psu month[−1] during boreal winter through summer and OSCAR currents give freshening of <0.2 psu month[−1] throughout the year (Figure 8a). The W region is relatively well sampled by surface drifters in comparison to

the rest of the tropical North Atlantic (LG05), giving confidence to the drifter-based climatologies in this region.

[35] In the N region the differences between advection estimates are similar in magnitude to the residual, suggesting that horizontal advection may be an important source of uncertainty. In the S region the differences in advection are similar to those in the N region (~0.05 psu month[−1]), whereas the magnitude of the residual is much larger (~0.2 psu month[−1] during boreal fall/winter). In this region it is therefore unlikely that errors in horizontal advection account for a significant portion of the discrepancies in the salinity balance.

4.2. Interpretation in Terms of Physical Processes

[36] It is also possible that unresolved physical processes contribute significantly to the residual in each region during boreal fall/winter. Among the possibilities is vertical turbulent mixing, which involves both turbulent entrainment and diffusion. The combination of these processes may have a significant effect on SSS, given the presence of a thick barrier layer (i.e., subsurface source of high salinity) during these seasons (Figure 1b). In the following paragraphs we interpret the residuals in terms of entrainment, recognizing that diffusive processes, which we cannot explicitly determine, may also be involved.

[37] On the basis of *Kraus and Turner*'s [1967] one-dimensional thermocline model, mixed layer deepening (i.e., entrainment velocity >0) occurs when the combination of wind and surface buoyancy forcing results in a net generation of turbulent kinetic energy in the mixed layer. The surface buoyancy flux is defined as $B = B_h + B_w$, where
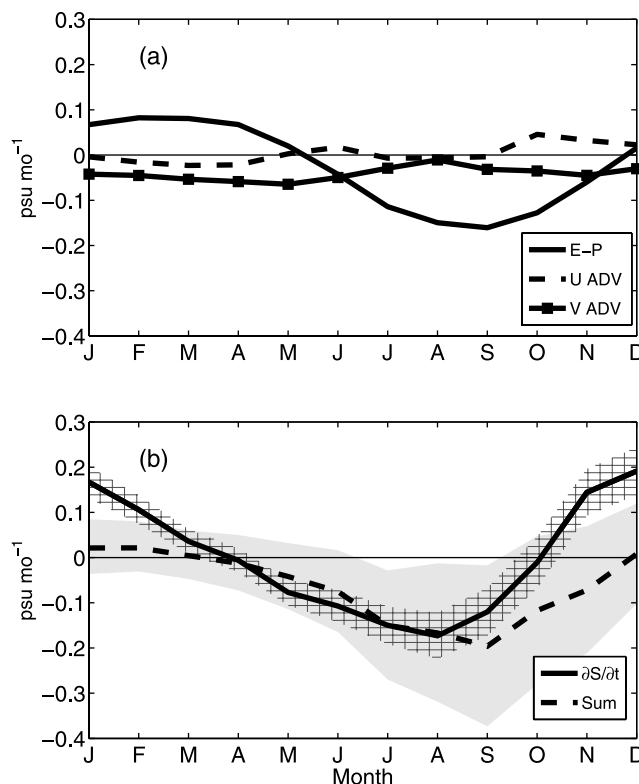

Figure 7. Same as in Figure 4 except for the S region (see Figure 3a for bounds of the region).
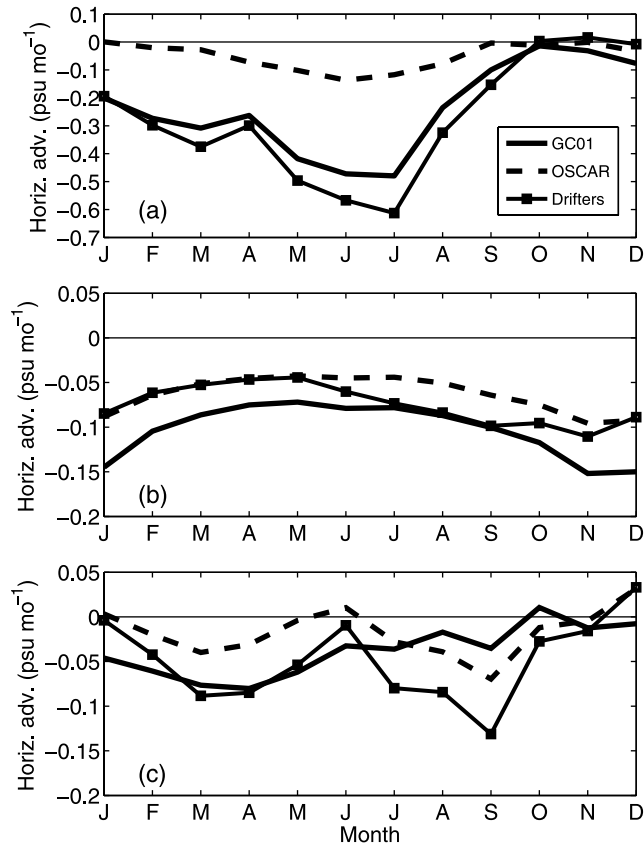
Figure 8. (a) Horizontal salinity advection in the W region estimated using GC01 currents (solid), OSCAR currents (dashed), and LG05 currents (squares). (b) Same as Figure 8a except for N region. (c) Same as Figure 8a except for S region.

$B_h = \alpha c_p^{-1} Q$ is the component due to the surface heat flux and $B_w = \beta \rho S(P - E)$ is the component due to the freshwater flux. Here α is the coefficient of thermal expansion of seawater, c_p is the heat capacity, Q is the surface heat flux (shortwave radiation + latent heat loss + net longwave radiation emission + sensible heat loss), and β is the coefficient of haline contraction. Throughout most of the tropical North Atlantic wind speed reaches a maximum in boreal winter (Figure 9a). In contrast, the surface buoyancy flux reaches a distinct minimum in December and January, with a net loss of buoyancy in the W and N regions during these months (Figure 9b). The strong seasonal cycle results primarily from changes in B_h (the peak-to-peak amplitude of B_w is <2 mg m^{-2} s^{-1} in all three regions). The combination of strong winds and weak buoyancy flux during boreal winter should cause the mixed layer to deepen in all three regions (Figure 9c). In the absence of horizontal mass divergence, the positive MLD tendency, in combination with an increase in salinity with depth at the base of the mixed layer (Figure 9d), would act to increase mixed layer salinity.

[38] In an attempt to quantify the contributions from entrainment in the W, N, and S regions, we consider a three-dimensional expression for entrainment velocity, w_e, given by

$$w_e = H(\partial h / \partial t + \nabla \cdot h\mathbf{v}) \qquad (2)$$

where H is the Heaviside unit function ($H = 0$ when the term in parentheses is <0 and $H = 1$ otherwise) [*Stevenson and Niiler*, 1983]. Following *Moisan and Niiler* [1998] entrainment is defined as $(\Delta S)w_e h^{-1}$, where $\Delta S = S - S_{-h}$. We use monthly climatological BM07 MLD and GC01 $\mathbf{v}$ to estimate the terms in (2) and WOA01 salinity to estimate ΔS. Results are similar if ML97 MLD and OSCAR or LG05 currents are used.

[39] However, in all three regions the magnitude of the divergence term in (2) is <0 throughout the year in all three regions and therefore tends to decrease the magnitude of entrainment during boreal fall/winter, when $\partial h/\partial t > 0$. The magnitude of the divergence term is at most 30% that of $\partial h/\partial t$ so that our estimate of entrainment is determined pri-

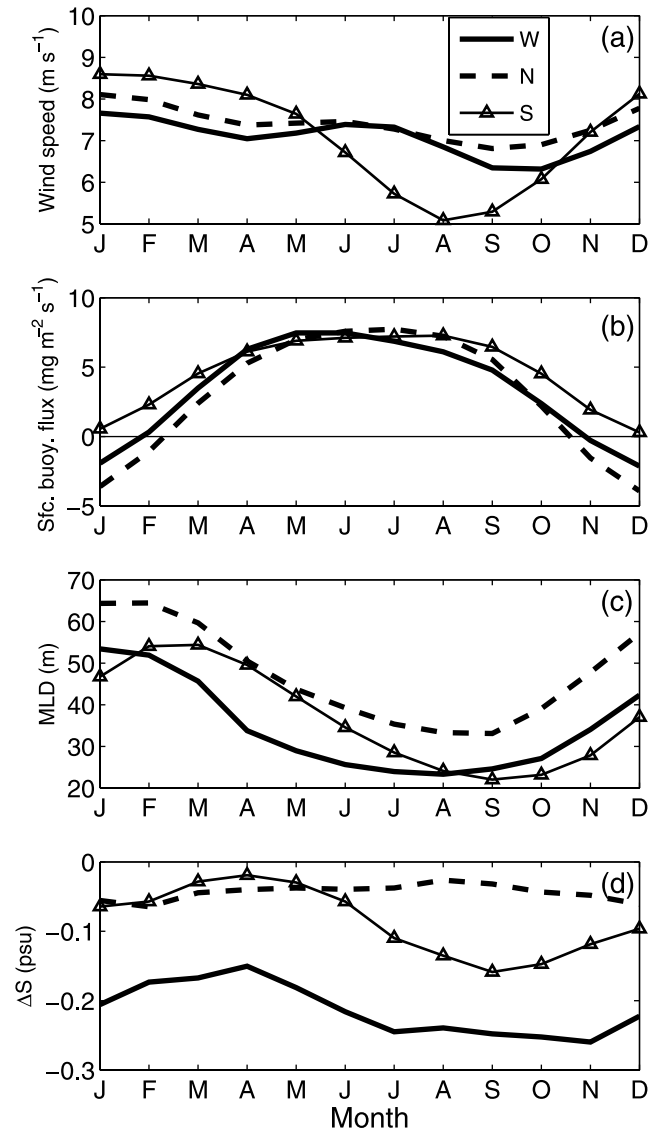**Figure 9.** (a) NCEP/DOE reanalysis-2 (NCEP2) wind speed averaged in the W (solid), N (dashed), and S (triangles) regions. (b) Same as Figure 9a except for net surface buoyancy flux. Values >0 indicate buoyancy flux into the ocean. (c) Same as Figure 9a except for mixed layer depth. (d) Same as Figure 9a except for the difference between mixed layer salinity and salinity at the base of the mixed layer (ΔS).
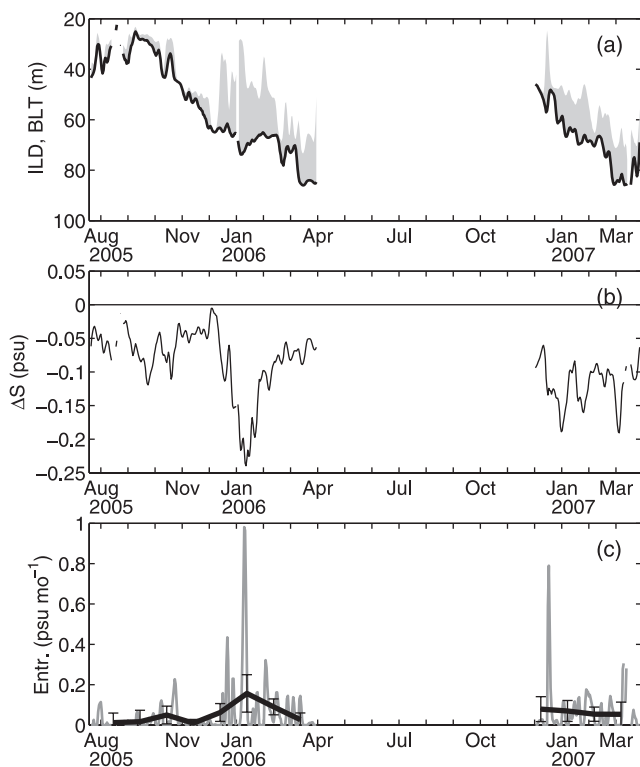
Figure 10. (a) Isothermal layer depth (solid line) and barrier layer thickness (shading), estimated from daily PIRATA subsurface temperature and salinity at 15°N, 38°W. (b) Difference between mixed layer salinity and salinity at the base of the mixed layer (ΔS) and (c) entrainment at the same location. All time series have been smoothed with two passes of a 3-d running mean filter. Bold line in Figure 10c is monthly averaged entrainment estimated from daily values. Vertical bars are one standard error (described in Appendix A).

marily by increases in mixed layer depth. Entrainment calculated from (2) using monthly climatological data, however, is <0.03 psu month^{-1} in the N and S regions and <0.05 psu month^{-1} in the W region. These values are much smaller than the residuals of our balances. Only positive entrainment velocities (i.e., mixed layer deepening) contribute to changes in mixed layer salinity, so it is possible that high-frequency fluctuations of h and ΔS (period <2 months), which are not captured by the monthly mean climatologies, may be important. We therefore estimate entrainment using daily averaged PIRATA subsurface temperature and salinity measurements at 15°N, 38°W (Figure 3a shows the mooring location in relation to the averaging regions). We restrict our analysis to the period July 2005 to March 2007 when salinity was measured at 1, 10, 20, 40, 60, and 120 m since the coarser vertical resolution of the moored salinity measurements in earlier records leads to significant uncertainties in the estimation of h and ΔS. Data during April–November 2006 are excluded from the analysis because of the presence of unrealistic salinity drifts at 20 m and 40 m, which limit the usable record lengths to ~12 months. We estimate ΔS and h from daily subsurface temperature and salinity at the mooring using the criterion of a 0.07 kg m^{-3} density increase from a depth of 10 m as in BM07.

[40] Daily measurements from the PIRATA mooring at 15°N suggest that entrainment may play an important role in the mixed layer salinity balance of the tropical North Atlantic. Entrainment reaches a peak of ~0.15 psu month^{-1} in January 2006, about three times the maximum value of entrainment estimated using monthly climatological h and ΔS (Figure 10c). The seasonal cycle of entrainment is well correlated with the seasonal cycle of barrier layer thickness (Figures 1b, 1d, and 10a). A thicker barrier layer generally corresponds to a sharper vertical salinity gradient at the base of the mixed layer, which increases the magnitude of ΔS (Figure 10b).

[41] Almost all of the entrainment at the mooring location is caused by deepening of the mixed layer on timescales of less than 2 months. Entrainment estimated from monthly climatological mixed layer depth is much weaker in comparison since it does not account for these high-frequency fluctuations. Maximum monthly values of entrainment are an order of magnitude smaller (<0.01 psu month^{-1}) when monthly climatological h, ΔS from the moorings are used instead of daily values. During boreal winter the barrier layer is thick (up to 40 m) and there are significant high-frequency fluctuations of mixed layer depth (Figure 10a). Each time the mixed layer deepens the barrier layer erodes, inducing a positive flux of salt into the mixed layer. The peak of entrainment in January 2006 corresponds to a significant increase in ΔS in the presence of strong mixed layer depth and barrier layer thickness fluctuations.

[42] The seasonal cycle of entrainment at the PIRATA location corresponds reasonably well with the storage-minus-sum residuals averaged in the N and S regions. In addition, there are some similarities between our results and those of *Foltz et al.* [2004], which are based on data from the PIRATA moorings along 38°W but which were not analyzed for high-frequency fluctuations of entrainment. *Foltz et al.* [2004] showed a discrepancy between the mixed layer salt storage rate and the sum of the forcing terms at 15°N that implied a missing source of salt during most of the year, consistent with our area-averaged residuals and our estimates of entrainment at this location.

[43] It is also possible that horizontal eddy advection may contribute significantly to the salinity balance of the tropical North Atlantic. We anticipate that this term will be most important in the W region, where there are significant horizontal salinity gradients in the presence of strong intra-seasonal variations of surface velocity (~50 cm s^{-1} [e.g., *Johns et al.*, 1990; *Richardson et al.*, 1994; *Fratantoni and Glickson*, 2002]). In a numerical modeling study, *Ferry and Reverdin* [2004] concluded that eddy advection plays only a minor role in the evolution of interannual SSS anomalies in the western tropical North Atlantic in comparison to large-scale horizontal advection and entrainment. However, it is unclear how these results translate to the seasonal cycle. In addition, *Ferry and Reverdin* [2004] noted that their model produced too few retroflection eddies, implying that experiments with a higher horizontal resolution will likely be required to accurately assess the role of eddy advection in the western basin.

5. Summary and Discussion

[44] This study attempts to diagnose the seasonal cycle of mixed layer salinity in the tropical North Atlantic from a

variety of satellite and in situ data sets. Within the error bars of our calculations, we have found that changes in mixed layer salinity during most of the year and throughout most of the basin are balanced by a combination of horizontal salinity advection, evaporation, and precipitation.

[45] The western tropical North Atlantic (10–25°N, 50–65°W) exhibits a pronounced seasonal cycle of surface salinity that is driven primarily by changes in horizontal salinity advection. Mixed layer salinity decreases during boreal spring and summer in response to the northwestward advection of low-salinity water from the Amazon. Horizontal transport peaks in June–July, roughly 1 month after the peak outflow from the Amazon. Increases in salinity during the remainder of the year are associated with a reduction in the transport of low-salinity water from the southeast.

[46] In the northern tropical Atlantic (15–25°N, 20–50°W), changes in the surface moisture flux are balanced by changes in meridional advection, resulting in a very weak seasonal cycle of mixed layer salinity. Farther south (5–15°N, 20–45°W) seasonal variations of precipitation are stronger. There is a period of significant freshening during boreal summer and fall, when the ITCZ is farthest north, and an increase in salinity during boreal winter, when evaporation exceeds precipitation.

[47] The sum of the monthly averaged forcing terms (E−P and horizontal advection) underestimates the mixed layer salinity tendency in all three regions during boreal fall and winter. During these seasons there is a maximum in surface wind speed and a minimum in surface buoyancy flux throughout the tropical North Atlantic. The in-phase relationship between these sources and sinks of turbulent kinetic energy should result in a deepening of the mixed layer during boreal fall and winter. The mixed layer deepening occurs in the presence of a sharp vertical salinity gradient at the base of the mixed layer, suggesting that vertical entrainment may explain a significant portion of the residual. Daily measurements from a PIRATA mooring in the central tropical North Atlantic are consistent with this interpretation, revealing high-frequency fluctuations of mixed layer depth and the vertical salinity gradient at the base of the mixed layer (ΔS) that together generate a significant vertical flux of salt into the mixed layer. These fluctuations are not captured by monthly climatologies.

[48] Our results generally agree with those of *Foltz et al.* [2004]. Their study is based on similar SSS and mixed layer velocity climatologies, together with measurements from PIRATA moorings along 38°W. They also found that meridional advection and E−P dominate in the central tropical North Atlantic (15°N and 12°N) and that precipitation dominates farther south (8°N). *Foltz et al.* [2004] used monthly climatological mixed layer depth and ΔS to estimate entrainment at each PIRATA location and found that it contributed insignificantly to the mixed layer salinity balance. In this study we used daily estimates based on measurements from the PIRATA mooring at 15°, 38°W and found that entrainment plays a more significant role, especially during boreal fall and winter. These results may at least partially account for the missing source of salinity in the balance estimated by *Foltz et al.* [2004] at 15°N.

[49] There are significant uncertainties associated with our estimates of horizontal salinity advection and entrainment. Errors in salinity advection are caused by a combi-

nation of uncertainties in mixed layer depth, horizontal SSS gradients, and mixed layer velocity. Vertical temperature and salinity profiles from Argo and satellite-based SSS estimates from Aquarius [*Koblinsky et al.*, 2003] will help to reduce uncertainties in mixed layer depth and SSS, respectively. There are also uncertainties in the estimates of the surface moisture flux, which rely primarily on measurements from satellites. Continued in situ measurements of precipitation at the PIRATA mooring locations will help to quantify these uncertainties.

[50] The introduction in July 2005 of 10 m velocity measurements at several locations in the PIRATA array will help to assess uncertainties in mixed layer velocity analyses and to reduce uncertainties in the estimation of horizontal salinity advection. Additional salinity measurements at 10 m and 60 m, begun at these same PIRATA sites in July 2005, will help to better define the mixed layer depth and ΔS. Even higher resolution measurements (5 m) of temperature and salinity in the upper 100 m at these sites would be desirable for 1−2 years to improve our estimates.

[51] Finally, we have neglected horizontal eddy advection, which may contribute significantly to the salinity balance of the tropical North Atlantic. We anticipate that this term will be most important in the western basin, where there are significant horizontal salinity gradients in the presence of strong intraseasonal variations of surface velocity. The current observational network of surface velocity and SSS measurements is inadequate for reliably estimating eddy advection. Well-designed, high-resolution, numerical modeling experiments hold the most promise for quantification of this term.

[52] The results of this study suggest that the mixed layer salinity balance of the tropical North Atlantic Ocean results from the complex interplay of surface fluxes, horizontal advection, and vertical entrainment. However, there are significant uncertainties associated with the estimation of these processes, especially horizontal advection and entrainment, that limit our ability to accurately diagnose seasonal sea surface salinity variability in this region. Improved understanding of the seasonal cycle, which is by far the strongest source of surface salinity variability in the tropical North Atlantic, will depend on continued improvements in surface flux estimates as well as continued measurements of mixed layer currents and subsurface salinity to augment future satellite-based sea surface salinity observations.

Appendix A: Objective Analysis and Error Estimates

[53] Because of limitations in sampling frequency, we have found that a simple gridded SSS analysis is noisy in space and contains some monthly grid boxes with no data. We therefore apply a Kriging objective analysis technique to the individual SSS observations to produce smoother maps and to fill regions devoid of data. This method assumes that the covariance function of SSS depends only on the separation of two data points and finds a local estimate based on a weighted average of all values within a specified search radius.

[54] Kriging is performed on a 2.5° × 2.5° mesh using the EasyKrig3.0 software available from http://globec.whoi.edu/software/kriging/easy_krig/easy_krig.html. We first calcu-

late an empirical semivariogram using all available measurements ($\gamma_e(r) = C(r = 0) - C(r)$, where $\gamma_e(r)$ is the semivariogram at a separation distance r and C is the covariance). We then fit γ_e to a smooth exponential function

$$\gamma(r) = (s - n)\left[1 - e^{-\left(\frac{r}{L}\right)^p}\right] + n \qquad (A1)$$

where γ is the modeled semivariogram, normalized by the variance ($C(r = 0)$), for a separation distance r; s is the "sill" (maximum value of the semivariogram for large separation distances) corrected for the "nugget effect" (n, which accounts for measurement error). The length scale (L) and power (p) determine the shape of the semivariogram (i.e., the decorrelation length scale and the manner in which the covariance decreases with increasing r). We use the following values for the parameters in (A1), based on a least squares fit to the empirical semivariogram: $s = 0.92$, $n = 0.012$, $L = 0.05$, and $p = 1.26$. We note, however, that the results presented in this paper are not highly sensitive to reasonable changes in these parameters.

[55] Our error analysis takes into account uncertainties in the estimation of each term in the salinity equation (1). We first estimate errors for each climatological calendar month in each $2.5° \times 2.5°$ grid box. Monthly errors in SSS (ϵ_S) and mixed layer depth (ϵ_h) are estimated as one standard error of all available observations for each calendar month. Measurement errors are ignored since they are generally about an order of magnitude smaller than sampling errors, which are $\sim 0.04–0.2$ psu. Errors in horizontal mixed layer currents ($\epsilon_{u,v}$) are difficult to quantify because there are no long-term moored current records in the tropical North Atlantic for comparison. For simplicity, we therefore assume an optimistic error in both velocity components of 5 cm s^{-1}. Errors in mixed layer salinity tendency are then estimated as $\epsilon_{\partial S/\partial t} = \left(\sqrt{\epsilon_{S_{t+1}}^2 + \epsilon_{S_{t-1}}^2}\right)/\Delta t$, where $\Delta t = 2$ months. Errors in zonal salinity advection are estimated as $\epsilon_{uadv} = \sqrt{\epsilon_u^2(\partial S/\partial x)^2 + u^2\epsilon_{\partial S/\partial x}^2}$, with an analogous expression for ϵ_{vadv}. Here $\epsilon_{\partial S/\partial x} = \left(\sqrt{\epsilon_{S_{x+1}}^2 + \epsilon_{S_{x-1}}^2}\right)/\Delta x$, with $\Delta x = 5°$. Here we have assumed that the errors for different quantities are uncorrelated.

[56] The methodology described above gives error estimates for the mixed layer salinity storage rate, horizontal advection, and entrainment in each $2.5°$ grid box. To estimate errors for each region shown in Figure 3a, we follow *Smith et al.* [1994] and estimate the degrees of freedom for each area-averaged quantity as

$$dof = N\left[\sum_{i=1}^{N}\sigma_i^2\right]\left[\sum_{i=1}^{N}\sigma_i^2 + 2\sum_{i=1}^{N-1}\sum_{j=i+1}^{N}cov(x_i, x_j)\right]^{-1} \qquad (A2)$$

Here σ_i^2 is the variance at grid box i, N is the number of grid boxes in a given averaging region, and $cov(x_i, x_j)$ is the covariance between the quantity in grid boxes i and j. For the extreme case in which the time series in each pair of grid boxes are uncorrelated, $dof = N$, and when the time series are perfectly correlated, $dof = 1$. Using (A2), monthly

climatological errors for the area-averaged quantities are estimated as

$$\epsilon_{ave} = \frac{1}{dof}\sqrt{\frac{dof}{N}\sum_{i=1}^{N}\epsilon_i^2} \qquad (A3)$$

where ϵ_i is the error for grid box i.

[57] Error estimates for the monthly *Yu et al.* [2004] evaporation and GPCP precipitation analyses are based on comparisons to measurements from the PIRATA moorings at 8°N, 12°N, and 15°N along 38°W. Daily averaged precipitation is available directly from the moorings, while evaporation is estimated from daily buoy air temperature, relative humidity, SST, and wind speed using a bulk algorithm [*Fairall et al.*, 2003]. We form monthly averages from the daily PIRATA precipitation and evaporation estimates and estimate errors for each calendar month as the RMS difference between the monthly *Yu et al.* [2004] and GPCP analyses and the corresponding monthly PIRATA estimates. This gives error estimates only at the four buoy locations along 38°W. Errors for each of the averaging regions are estimated as follows. For the W and N regions we use the error estimates at 15°N, 38°W, and for the S region we use the mean of the errors at 12°N and 8°N. These precipitation error estimates likely overestimate the true errors since they assume that the moored rain gauges are error-free. In addition, errors may be overestimated because the comparison does not account for the different spatial sampling of the GPCP rainfall estimates, which are area averages, and the PIRATA measurements, which are from single locations. Nonetheless, typical errors inferred for in E−P are relatively small (<0.02 psu month^{-1} for the W and S regions and <0.005 psu month^{-1} for the N region) in comparison to those for horizontal advection (~ 0.1 for the W and S regions and ~ 0.02 for the N region).

[58] There are significant uncertainties associated with our estimation of errors for horizontal mixed layer salinity advection, evaporation, and precipitation. In addition to the formal error analysis described above we have therefore provided a comparison of several different horizontal velocity, evaporation, and precipitation products to further quantify uncertainties in the mixed layer salinity balance (see section 4).

[59] In order to assess errors in daily entrainment estimated from the PIRATA mooring at 15°N, 38°W we make use of high-vertical-resolution (<5 m) temperature and salinity profiles from the World Ocean Database 2001 (WOD01) as follows. First WOD01 temperature and salinity profiles in the tropical North Atlantic (5–25°N, 20–65°W) are resampled to the measurement depths of the mooring temperature and salinity using linear interpolation. We then estimate h and ΔS from the original WOD01 profiles (h_o, ΔS_o) and from the resampled profiles (h_r, ΔS_r). The differences between h_o and h_r and between ΔS_o and ΔS_r give estimates of the errors associated with calculating h and ΔS from the limited vertical resolution available at the moorings. We collect h_o, ΔS_o, h_r, and ΔS_r into 3 m vertical bins based on the value of h_r. We then use the RMS differences between h_o and h_r and between ΔS_o and ΔS_r in each vertical bin to estimate the errors associated with the daily mooring h and ΔS. We also add to the mooring-based

h and ΔS the mean $h_o - h_r$ and $\Delta S_o - \Delta S_r$. Typical errors in h and ΔS are 5 m and 0.03 psu, respectively. Typical values of $h_o - h_r$ and $\Delta S_o - \Delta S_r$ are 5 m and 0.005 psu, respectively.

[60] The number of degrees of freedom for the daily time series of h and ΔS is then estimated as

$$dof = \left[\sum_{i=0}^{25} \sigma_i^2 \right] \left(\frac{1}{N} \right) \qquad (A4)$$

Here N is the number of days and σ_i is the autocorrelation at lag i. Error estimates for monthly averaged entrainment from the mooring are then estimated as in (A3).

References

Adler, R. F., et al. (2003), The Version 2 Global Precipitation Climatology Project (GPCP) monthly precipitation analysis (1979-present), *J. Hydrometeorol.*, 4, 1147–1167.

Bonjean, F., and G. S. E. Lagerloef (2002), Diagnostic model and analysis of the surface currents in the tropical Pacific Ocean, *J. Phys. Oceanogr.*, 32, 2938–2954.

Boyer, T. P., C. Stephens, J. I. Antonov, M. E. Conkright, R. A. Locarnini, T. D. O'Brien, and H. E. Garcia (2002), *World Ocean Atlas 2001, vol. 2, Salinity, NOAA Atlas NESDIS 50*, edited by S. Levitus, 165 pp., U.S. Govt. Print. Off., Washington, D. C.

Conkright, M. E., et al. (2002), *World Ocean Database 2001, vol. 1, Introduction, NOAA Atlas NESDIS 42*, edited by S. Levitus, 167 pp., U.S. Govt. Print. Off., Washington, D. C.

Cronin, M. F., and M. J. McPhaden (1998), Upper ocean salinity balance in the western equatorial Pacific, *J. Geophys. Res.*, 103, 27,567–27,588.

Dai, A. G., and K. E. Trenberth (2002), Estimates of freshwater discharge from continents: Latitudinal and seasonal variations, *J. Hydrometeorol.*, 3, 660–687.

de Boyer Montégut, C., J. Mignot, A. Lazar, and S. Cravatte (2007), Control of salinity on the mixed layer depth in the world ocean: 1. General description, *J. Geophys. Res.*, 112, C06011, doi:10.1029/2006JC003953.

Delcroix, T., and C. Hénin (1991), Seasonal and interannual variations of sea surface salinity in the tropical Pacific Ocean, *J. Geophys. Res.*, 96, 22,135–22,150.

Delcroix, T., C. Hénin, V. Porte, and P. Arkin (1996), Precipitation and sea-surface salinity in the tropical Pacific Ocean, *Deep Sea Res., Part I*, 43, 1123–1141.

Delcroix, T., M. J. McPhaden, A. Dessier, and Y. Gouriou (2005), Time and space scales for sea surface salinity in the tropical oceans, *Deep Sea Res., Part I*, 52, 787–813.

Dessier, A., and J. R. Donguy (1994), The sea surface salinity in the tropical Atlantic between 10°S and 30°N—seasonal and interannual variations (1977–1989), *Deep Sea Res., Part I*, 41, 81–100.

Fairall, C. W., E. F. Bradley, J. E. Hare, A. A. Grachev, and J. B. Edson (2003), Bulk parameterization of air-sea fluxes: Updates and verification for the COARE algorithm, *J. Clim.*, 16, 571–591.

Ferry, N., and G. Reverdin (2004), Sea surface salinity interannual variability in the western tropical Atlantic: An ocean general circulation model study, *J. Geophys. Res.*, 109, C05026, doi:10.1029/2003JC002122.

Ffield, A. (2007), Amazon and Orinoco River plumes and NBC rings: Bystanders or participants in hurricane events?, *J. Clim.*, 20, 316–333.

Foltz, G. R., S. A. Grodsky, J. A. Carton, and M. J. McPhaden (2004), Seasonal salt budget of the northwestern tropical Atlantic Ocean along 38°W, *J. Geophys. Res.*, 109, C03052, doi:10.1029/2003JC002111.

Fratantoni, D. M., and D. A. Glickson (2002), North Brazil Current ring generation and evolution observed with SeaWiFS, *J. Phys. Oceanogr.*, 32, 1058–1074.

Freitag, H. P., M. E. McCarty, C. Nosse, R. Lukas, M. J. McPhaden, and M. F. Cronin (1999), COARE Seacat data: Calibrations and quality control procedures, *NOAA Tech. Memo., ERL PMEL-115*, 89 pp.

Giannini, A., R. Saravanan, and P. Chang (2003), Oceanic forcing of Sahel rainfall on interannual to interdecadal time scales, *Science*, 302, 1027–1030.

Goldenberg, S. B., C. W. Landsea, A. M. Mestaz-Nunez, and W. M. Gray (2001), The recent increase in Atlantic hurricane activity: Causes and implications, *Science*, 293, 474–479.

Grodsky, S. A., and J. A. Carton (2001), Intense surface currents in the tropical Pacific during 1996–1998, *J. Geophys. Res.*, 106, 16,673–16,684.

Hastenrath, S., and L. Greischar (1993), Circulation mechanisms related to Northeast Brazil rainfall anomalies, *J. Geophys. Res.*, 98, 5093–5102.

Hénin, C., and J. Grelet (1996), A merchant ship thermosalinograph network in the Pacific Ocean, *Deep Sea Res., Part I*, 43, 1833–1856.

Johns, W. E., T. N. Lee, F. A. Schott, R. J. Zantopp, and R. H. Evans (1990), The North Brazil Current retroflection: Seasonal structure and eddy variability, *J. Geophys. Res.*, 95, 22,103–22,120.

Johnson, E. S., G. S. E. Lagerloef, J. T. Gunn, and F. Bonjean (2002), Surface salinity advection in the tropical oceans compared with atmospheric freshwater forcing: A trial balance, *J. Geophys. Res.*, 107(C12), 8014, doi:10.1029/2001JC001122.

Johnson, E. S., F. Bonjean, G. S. E. Lagerloef, J. T. Gunn, and G. T. Mitchum (2007), Validation and error analysis of OSCAR sea surface currents, *J. Atmos. Oceanic Technol.*, 24, 688–701.

Kanamitsu, M., W. Ebisuzaki, J. Woollen, S. K. Yang, J. J. Hnilo, M. Fiorino, and G. L. Potter (2002), NCEP-DOE AMIP-II reanalysis (R-2), *Bull. Am. Meteorol. Soc.*, 83, 1631–1643.

Koblinsky, C. J., P. Hildebrand, D. LeVine, F. Pellerano, Y. Chao, W. Wilson, S. Yueh, and G. Lagerloef (2003), Sea surface salinity from space: Science goals and measurement approach, *Radio Sci.*, 38(4), 8064, doi:10.1029/2001RS002584.

Kraus, E. B., and J. S. Turner (1967), A one-dimensional model of the seasonal thermocline, *Tellus*, 19, 98–105.

Lamb, P. J. (1978), Large-scale tropical Atlantic surface circulation patterns associated with sub-Saharan weather anomalies, *Tellus*, 30, 240–251.

Latif, M., N. Keenlyside, and J. Bader (2007), Tropical sea surface temperature, vertical wind shear, and hurricane development, *Geophys. Res. Lett.*, 34, L01710, doi:10.1029/2006GL027969.

Lukas, R., and E. Lindstrom (1991), The mixed layer of the western equatorial Pacific Ocean, *J. Geophys. Res.*, 96, suppl., 3343–3357.

Lumpkin, R., and S. L. Garzoli (2005), Near-surface circulation in the tropical Atlantic Ocean, *Deep Sea Res., Part I*, 52, 495–518.

Maes, C., K. Ando, T. Delcroix, W. S. Kessler, M. J. McPhaden, and D. Roemmich (2006), Observed correlation of surface salinity, temperature and barrier layer at the eastern edge of the western Pacific warm pool, *Geophys. Res. Lett.*, 33, L06601, doi:10.1029/2005GL024772.

Moisan, J. R., and P. P. Niiler (1998), The seasonal heat budget of the North Pacific: Net heat flux and heat storage rates (1950–1990), *J. Phys. Oceanogr.*, 28, 401–421.

Monterey, G. I., and S. Levitus (1997), *Seasonal Variability of Mixed Layer Depth for the World Ocean, NOAA Atlas NESDIS 14*, 5 pp., 87 figures, U.S. Govt. Print. Off., Washington, D. C.

Muller-Karger, F. E., C. R. McClain, and P. L. Richardson (1988), The dispersal of the Amazon's water, *Nature*, 333, 56–58.

Pailler, K., B. Bourles, and Y. Gouriou (1999), The barrier layer in the western tropical Atlantic Ocean, *Geophys. Res. Lett.*, 26, 2069–2072.

Rao, R. R., and R. Sivakumar (2003), Seasonal variability of sea surface salinity and salt budget of the mixed layer of the north Indian Ocean, *J. Geophys. Res.*, 108(C1), 3009, doi:10.1029/2001JC000907.

Reverdin, G., D. Cayan, H. D. Dooley, D. J. Ellett, S. Levitus, Y. du Penhoat, and A. Dessier (1994), Surface salinity of the North Atlantic: Can we reconstruct its fluctuations over the last one hundred years?, *Prog. Oceanogr.*, 33, 303–346.

Richardson, P. L., G. E. Hufford, R. Limeburner, and W. S. Brown (1994), North Brazil Current retroflection eddies, *J. Geophys. Res.*, 99, 5081–5093.

Roemmich, D. (2000), The Argo project: Global ocean observations for understanding and prediction of climate variability, *Oceanography*, 13, 45–50.

Saunders, M. A., and A. R. Harris (1997), Statistical evidence links exceptional 1995 Atlantic hurricane season to record sea warming, *Geophys. Res. Lett.*, 24, 1255–1258.

Servain, J., A. J. Busalacchi, M. J. McPhaden, A. D. Moura, G. Reverdin, M. Vianna, and S. E. Zebiak (1998), A Pilot Research Moored Array in the Tropical Atlantic (PIRATA), *Bull. Am. Meteorol. Soc.*, 79, 2019–2031.

Shapiro, L. J., and S. B. Goldenberg (1998), Atlantic sea surface temperatures and tropical cyclone formation, *J. Clim.*, 11, 578–590.

Simmons, A. J., and J. K. Gibson (2000), *The ERA-40 project plan, Tech. Rep. ERA-40*, Eur. Cent. for Med.-Range Weather Forecasts, Reading, U.K.

Smith, T. M., R. W. Reynolds, and C. F. Ropelewski (1994), Optimal averaging of seasonal sea surface temperatures and associated confidence intervals (1860–1989), *J. Clim.*, 7, 949–964.

Sprintall, J., and M. Tomczak (1992), Evidence of the barrier layer in the surface layer of the tropics, *J. Geophys. Res.*, *97*, 7305–7316.

Stevenson, J. W., and P. P. Niiler (1983), Upper ocean heat budget during the Hawaii-to-Tahiti shuttle experiment, *J. Phys. Oceanogr.*, *13*, 1894–1907.

Vialard, J., and P. Delecluse (1998), An OGCM study for the TOGA decade. Part I: Role of salinity in the physics of the western Pacific fresh pool, *J. Phys. Oceanogr.*, *28*, 1071–1088.

Wong, A. P. S., G. C. Johnson, and W. B. Owens (2003), Delayed-mode calibration of autonomous CTD profiling float salinity data by theta-S climatology, *J. Atmos. Oceanic Technol.*, *20*, 308–318.

Worley, S. J., S. D. Woodruff, R. W. Reynolds, S. J. Lubker, and N. Lott (2005), ICOADS Release 2.1 data and products, *Int. J. Climatol.*, *25*, 823–842, doi:10.1002/joc.1166.

Xie, P. P., and P. A. Arkin (1997), Global precipitation: A 17-year monthly analysis based on gauge observations, satellite estimates, and numerical model outputs, *Bull. Am. Meteorol. Soc.*, *78*, 2539–2558.

Yin, X., A. Gruber, and P. Arkin (2004), Comparison of the GPCP and CMAP merged gauge-satellite monthly precipitation products for the period 1979–2001, *J. Hydrometeorol.*, *5*, 1207–1222.

Yu, L. S., R. A. Weller, and B. M. Sun (2004), Improving latent and sensible heat flux estimates for the Atlantic Ocean (1988–99) by a synthesis approach, *J. Clim.*, *17*, 373–393.

Zhang, Y., W. B. Rossow, A. A. Lacis, V. Oinas, and M. I. Mishchenko (2004), Calculation of radiative fluxes from the surface to top of atmosphere based on ISCCP and other global data sets: Refinements of the radiative transfer model and the input data, *J. Geophys. Res.*, *109*, D19105, doi:10.1029/2003JD004457.

————————————

G. R. Foltz, Joint Institute for the Study of the Atmosphere and Ocean, University of Washington, Seattle, WA 98195, USA. (gregory.foltz@noaa.gov)

M. J. McPhaden, Pacific Marine Environmental Laboratory, NOAA, 7600 Sand Point Way NE, Seattle, WA 98115, USA.